Journal of Materials Science: Materials in Electronics (2019) 30:20160–20165
https://doi.org/10.1007/s10854-019-02391-w

Phase compositions, microstructures, and microwave dielectric properties of $Li_2Zn_3Ti_4O_{12}$-based temperature stable materials modified by $CaTiO_3$ additions

Tingting Quan[1,2] · Guojin Shu[2] · Liang Hao[2] · Fancheng Meng[2]

Received: 1 May 2019 / Accepted: 15 October 2019 / Published online: 19 October 2019

Abstract
In present work, the microwave dielectric properties of $CaTiO_3$-added $Li_2Zn_3Ti_4O_{12}$ ceramics prepared by the conventional solid-state method have been investigated. The phase composition, microstructure and microwave dielectric properties of $(1-x)$ $Li_2Zn_3Ti_4O_{12}$–x $CaTiO_3$ ($x=3$, 4, 5, 6 and 7 wt%) ceramics were studied by X-ray diffraction (XRD), scanning electron microscopy (SEM), EDS and network analyzer. The XRD and EDS results indicated that the ceramics involved $Li_2Zn_3Ti_4O_{12}$ and $CaTiO_3$ phases. The SEM micrographs shown that as the $CaTiO_3$ contents increased, the average grain size of the composition ceramics decreased. The microwave dielectric properties of the composition ceramics can be effectively controlled by varying the $CaTiO_3$ contents. The values of dielectric constant (ε_r) and τ_f of the composition ceramics were increased, and the quality factor ($Q\times f$) was decreased with increasing the $CaTiO_3$ contents. Typically, a new temperature stable microwave dielectric material of 0.94 $Li_2Zn_3Ti_4O_{12}$–0.06 $CaTiO_3$ with excellent microwave dielectric properties of $\varepsilon_r=21.7$, $Q\times f=61{,}490$ GHz, and $\tau_f=+2.68$ ppm/°C was attained when sintered at 1175 °C for 4 h.

1 Introduction

The recent rapid advances in Internet of Things, the Industrial Internet, electronic warfare, intelligent transport systems and the fifth generation wireless systems. Microwave dielectric ceramics, as a key material used in these applications, have been received much more attention. It is known that miniaturization, integration, and high reliability are the important tendency in today's microwave electronic devices and portable terminals. Therefore, materials with high dielectric constant ($\varepsilon_r > 10$), high quality factor ($Q\times f \geq 10{,}000$ GHz) and near-zero temperature coefficient of resonant frequency ($|\tau_f| \leq 10$ ppm/°C) are strongly required. Especially, for the operating frequency in nowadays are increasing (e. g: Millimeter wave or submillimeter wave), materials with near-zero τ_f value become more and more critical [1–4].

In recent years, a great number of Li-containing compounds microwave dielectric ceramics with spinel-structure such as $Li_2MTi_3O_8$ (M = Mg, Zn, Co) [5, 6], $Li_2M_3Ti_4O_{12}$ (M = Zn, Mg, Co) [7–9] and $Li_2ZnTi_5O_{12}$ [10] etc., have been extensively studied due to their excellent microwave dielectric properties. Among in these ceramics, the $Li_2Zn_3Ti_4O_{12}$ ceramic based on Li_2O–ZnO–TiO_2 ternary systems have attracted much attention for low cost, light weight, eco-friendly of the raw materials and excellent microwave dielectric properties: $\varepsilon_r=20.6$, $Q\times f=106{,}700$ GHz and $\tau_f=-48$ ppm/°C when sintered at 1075 °C for 2 h [7]. Unfortunately, the negative τ_f value ($\tau_f=-48$ ppm/°C) prohibits its practical applications. Therefore, compensate the τ_f value near-zero simultaneously without much deteriorating the microwave dielectric properties is urgent. To achieve a near-zero τ_f for the $Li_2Zn_3Ti_4O_{12}$ ceramic, up till now, introducing a new material with an opposite τ_f value in the ceramic system has been demonstrated as an effective approach to adjust the τ_f value near-zero [11, 12]. Summarize previous works, $CaTiO_3$ have often been utilized as a τ_f compensation materials due to it's high positive τ_f

✉ Tingting Quan
18983225206@189.cn

✉ Fancheng Meng
mengfancheng@cqut.edu.cn

[1] Intelligent Manufacturing and Automobile School, Chongqing College of Electronic Engineering, Chongqing 401331, People's Republic of China

[2] College of Materials Science and Engineering, Chongqing University of Technology, Chongqing 400054, People's Republic of China

($\tau_f \sim +800$ ppm/°C) value and do not easily react at high temperature [13–17].

In this work, $CaTiO_3$ as a τ_f compensation material and mixture with $Li_2Zn_3Ti_4O_{12}$ ceramic to form the $(1-x)$ $Li_2Zn_3Ti_4O_{12}$–x $CaTiO_3$ ceramics system to achieve the τ_f value of $Li_2Zn_3Ti_4O_{12}$ ceramic near-zero. In addition, the phases, sintering behaviors, and microwave dielectric properties of (1-x) $Li_2Zn_3Ti_4O_{12}$–x $CaTiO_3$ ceramics were investigated systematically.

2 Experimental

The $Li_2Zn_3Ti_4O_{12}$ and $CaTiO_3$ powders were synthesized via the solid-state reaction route using analytical grade powders of Li_2CO_3 (AR, ≥ 99%, GuoYao Co. Ltd., Shanghai, China), ZnO (AR, ≥ 99%, Macklin Co. Ltd., Shanghai, China), TiO_2 (AR, ≥ 99%, Macklin Co. Ltd., Shanghai, China) and $CaCO_3$ (AR, ≥ 99%, Macklin Co. Ltd., Shanghai, China) as raw materials. Stoichiometric Li_2CO_3, ZnO, TiO_2 and $CaCO_3$ were mixed according to the formula of $Li_2Zn_3Ti_4O_{12}$ and $CaTiO_3$ with ZrO_2 balls by ball mill with ethanol for 4 h, respectively. The mixtures were dried and calcined at 1000 °C for 4 h to form $Li_2Zn_3Ti_4O_{12}$ and $CaTiO_3$ phase. Thereafter, The calcined powders were mixed according to the desired composition $(1-x)$ $Li_2Zn_3Ti_4O_{12}$–x $CaTiO_3$ ($x = 3$, 4, 5, 6 and 7 wt%) were mixed together and reground in ethanol medium for 4 h to get homogeneously mixture powders. After drying, the mixed powders were ground with 5 wt% polyvinyl alcohol (PVA) solution and then pelleted to 15 mm diameter and 7–8 mm thick disks at 5 MPa by hydraulic pressing. The thick disks samples were heated at 550 °C for 2 h to remove the organic binder and then sintered at 1100–1200 °C for 4 h in air at a heating rate of 5 °C/min.

The phases composition were identified by X-ray diffractometer (PANalytical Empyrean Series 2, UK) using CuKá radiation. The microstructures of sintered surfaces were performed by scanning electron microscope (SEM, JSM-6460LV, and Japan) coupled with energy-dispersive X-ray spectrometer (EDS, Philips). The bulk densities of the samples were measured by the Archimedes method. The ε_r and Q values were measured in the TE011 mode by using the Hakki-Coleman dielectric resonator method using a network analyzer (HP83752A, the United States) in a wide frequency (1–20 GHz).The temperature coefficients of resonant frequency (τ_f) were measured with changing temperatures from 20 to 60 °C defined as follows:

$$\tau_f = \left\{ (f_{60} - f_{20}) / (f_{20} \times 40) \right\} \times 10^6 (\text{ppm/°C})$$

where f_{20} and f_{60} represent the resonant frequency at 20 and 60 °C, respectively.

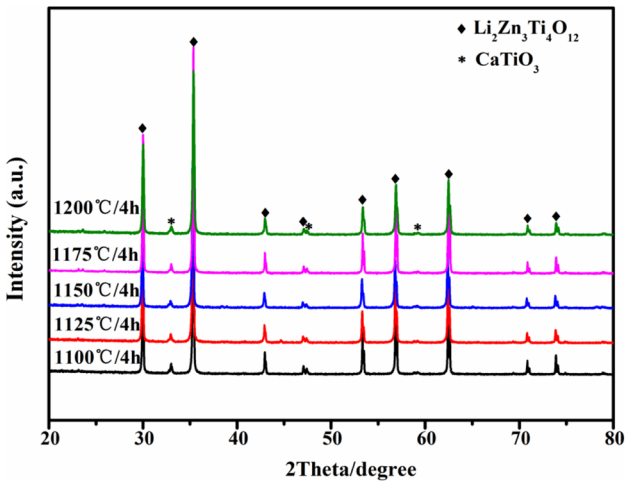

Fig. 1 X-ray diffraction patterns of 0.94 $Li_2Zn_3Ti_4O_{12}$–0.06 $CaTiO_3$ ceramics sintered at different temperatures for 4 h

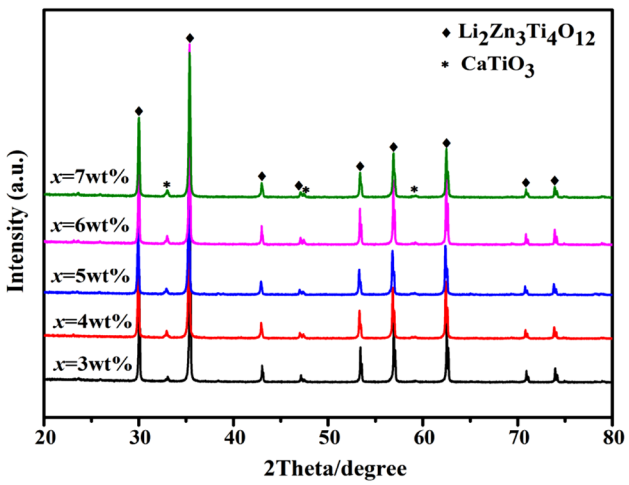

Fig. 2 X-ray diffraction patterns of $(1-x)$ $Li_2Zn_3Ti_4O_{12}$–x $CaTiO_3$ ceramics sintered at 1175 °C for 4 h with different x values

3 Results and discussion

The XRD results of 0.94 $Li_2Zn_3Ti_4O_{12}$–0.06 $CaTiO_3$ ceramics sintered at 1100–1200 °C for 4 h are given in Fig. 1. The peaks of the five-group samples indicating there are two phases co-exist in the 0.94 $Li_2Zn_3Ti_4O_{12}$–0.06 $CaTiO_3$ ceramics system, which including $Li_2Zn_3Ti_4O_{12}$ as the main crystalline phase (PDF # 44-10381) and $CaTiO_3$ as a minor phase (PDF # 42-0423), no other phases are detected. With the sintering temperatures increase from 1100 to 1200 °C, the peaks intensity changed not significantly. Figure 2 shows the XRD data of $(1-x)$ $Li_2Zn_3Ti_4O_{12}$–x $CaTiO_3$ ($3\ \text{wt\%} \le x \le 7\ \text{wt\%}$) ceramics sintered at 1175 °C for 4 h. The peaks intensity identified

gradually increased as x varies from 3 to 7 wt%, which corresponding to the increase of $CaTiO_3$ mass fraction in the mixture. These results indicated that the $CaTiO_3$ not only has a good compatibility with $Li_2Zn_3Ti_4O_{12}$ ceramic but also possible to adjust the τ_f value of $Li_2Zn_3Ti_4O_{12}$ ceramic near zero.

The typical SEM micrographs of 0.94 $Li_2Zn_3Ti_4O_{12}$–0.06 $CaTiO_3$ ceramics sintered at 1100–1200 °C for 4 h are displayed in Fig. 3. All of the micrographs show two types grain. As shown in Fig. 3a–c, with the sintering temperature increased, the microstructures become more compact and the amount of pores decreases when sintered at 1125 °C to 1150 °C, but not full-dense. As sintering temperature reaches 1175 °C, a homogeneous and dense microstructure is obtained (Fig. 3d). However, abnormal grain growth is observed at temperatures increases to 1200 °C. The SEM photographs of $(1-x)$ $Li_2Zn_3Ti_4O_{12}$–x $CaTiO_3$ (3 wt% $\leq x \leq$ 7 wt%) ceramics sintered at 1175 °C for 4 h are illustrated in Fig. 4. All photograph shows a homogeneous and compact microstructures, and the average grain size decreased as x increased from 3 to 7 wt%.

To further understand the crystal of the two grains mentioned in Fig. 3. The EDS results of 0.94 $Li_2Zn_3Ti_4O_{12}$–0.06 $CaTiO_3$ ceramics sintered at 1175 °C for 4 h are shown in Fig. 5. Grains with different shape and size are labeled as "spectrum 1" and "spectrum 2". From the EDS results, the "spectrum 1" grain are rich in Ca and Ti but poor in Zn, the "spectrum 2" grain are rich in Zn and Ti but poor in Ca. Combined with the XRD results shown in Fig. 1 and Fig. 2, the small cubic-shaped grains are $CaTiO_3$ phase and the large grains are $Li_2Zn_3Ti_4O_{12}$ phase.

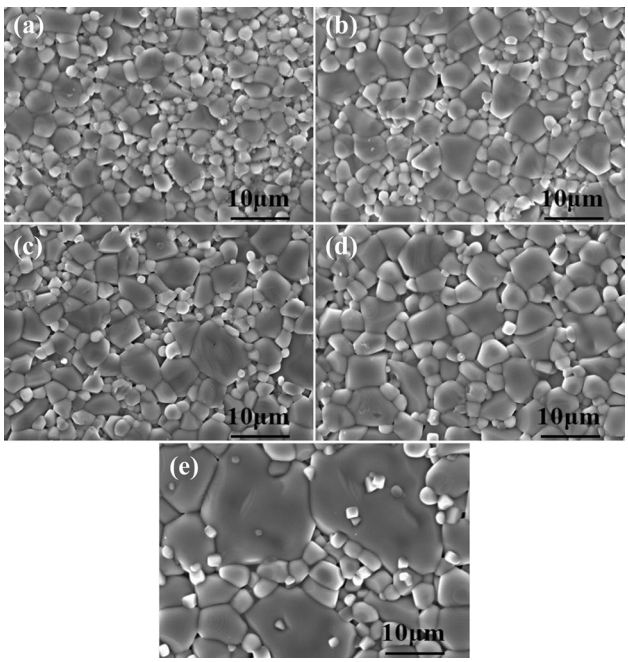

Fig. 3 SEM micrographs of $(1-x)$ $Li_2Zn_3Ti_4O_{12}$–x $CaTiO_3$ ceramics sintered for 4 h at different temperatures: **a** 1100 °C, **b** 1125 °C, **c** 1150 °C, **d** 1175 °C, and **e** 1200 °C

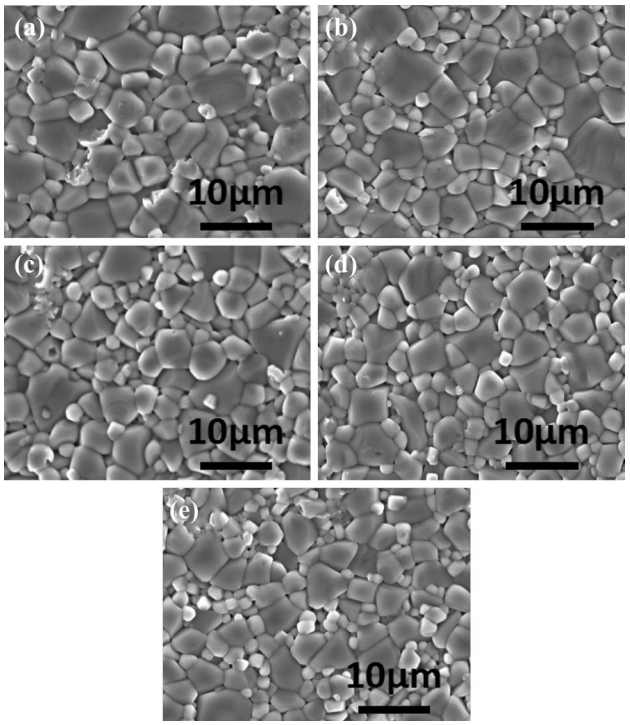

Fig. 4 SEM micrographs of $(1-x)$ $Li_2Zn_3Ti_4O_{12}$–x $CaTiO_3$ ceramics sintered at 1175 °C for 4 h: **a** $x=3$ wt%, **b** $x=4$ wt%, **c** $x=5$ wt%, **d** $x=6$ wt% and **e** $x=7$ wt%

Figure 6 shows the bulk densities of $(1-x)$ $Li_2Zn_3Ti_4O_{12}$–x $CaTiO_3$ (3 wt% $\leq x \leq$ 7 wt%) ceramics sintered at 1100–1200 °C for 4 h. With increasing sintering temperature, the bulk density of all sintered samples shown a trend of increasing during the sintering temperature rang from 1100 to 1175 °C, and reaching a maximum at 1175 °C. However, a slight decrease in density as the sintering temperature reaches 1200 °C, which possibly owing to the abnormal grain growth. Obviously, as the $CaTiO_3$ content increased, the bulk density of $(1-x)$ $Li_2Zn_3Ti_4O_{12}$–x $CaTiO_3$ (3 wt% $\leq x \leq$ 7 wt%) ceramics gradually decreases. The main reason may attributable to the difference in the theoretical density of $Li_2Zn_3Ti_4O_{12}$ ($\rho_{th}=4.3$ g/cm^3) and $CaTiO_3$ ($\rho_{th}=3.98$ g/cm^3).

The ε_r of $(1-x)$ $Li_2Zn_3Ti_4O_{12}$–x $CaTiO_3$ (3 wt% $\leq x \leq$ 7 wt%) ceramics sintered at 1100–1200 °C for 4 h are illustrated in Fig. 7. A same trend of ε_r and bulk density with sintering temperature is observed. With sintering temperature increasing from 1100 to 1175 °C, the ε_r values increased and reached a maximum at 1175 °C. However, when sintering temperature reaches 1200 °C, the ε_r values decreased. Furthermore, for the same temperature, the ε_r values of $(1-x)$ $Li_2Zn_3Ti_4O_{12}$–x $CaTiO_3$ (3 wt% $\leq x \leq$ 7 wt%)

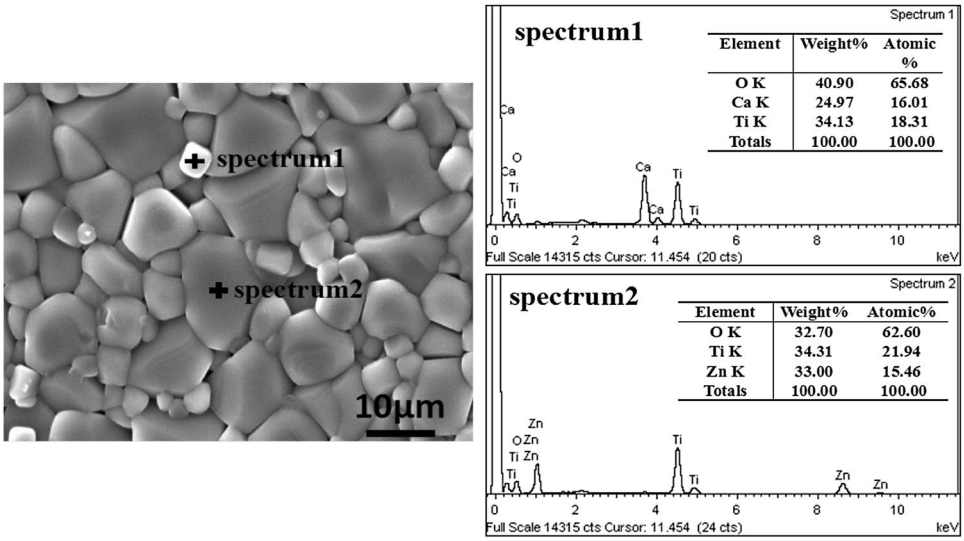

Fig. 5 The EDS results for the 0.94 $Li_2Zn_3Ti_4O_{12}$–0.06 $CaTiO_3$ ceramics sintered at 1175 °C for 4 h

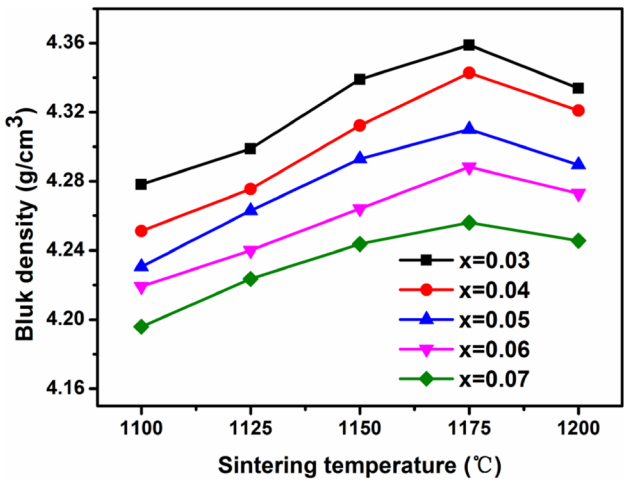

Fig. 6 Variation in the bulk density of $(1-x)$ $Li_2Zn_3Ti_4O_{12}$–x $CaTiO_3$ (3 wt% ≤ x ≤ 7 wt%) ceramics as a function of the sintering temperature

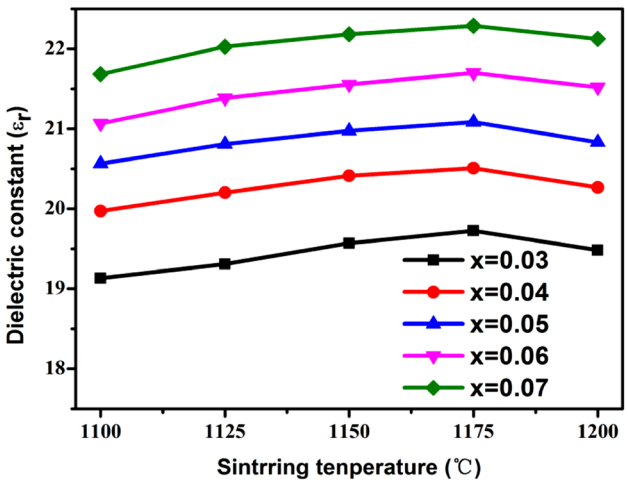

Fig. 7 Variation in the dielectric constant of the $(1-x)$ $Li_2Zn_3Ti_4O_{12}$–x $CaTiO_3$ (3 wt% ≤ x ≤ 7 wt%) ceramics as a function of sintering temperature

ceramics increased from 19.1 to 22.3 as the $CaTiO_3$ increased from 3 to 7 wt%, which due to $CaTiO_3$ has an ε_r ($\varepsilon_r \sim 170$) substantially greater than that of $Li_2Zn_3Ti_4O_{12}$ ($\varepsilon_r \sim 20.6$). Summary, the ε_r of $(1-x)$ $Li_2Zn_3Ti_4O_{12}$–x $CaTiO_3$ (3 wt% ≤ x ≤ 7 wt%) ceramics affected not only by the sintering temperature but also by the $CaTiO_3$ contents.

The Q × f values of $(1-x)$ $Li_2Zn_3Ti_4O_{12}$–x $CaTiO_3$ (3 wt% ≤ x ≤ 7 wt%) ceramics sintered at 1100–1200 °C for 4 h are presented in Fig. 8. As the sintering temperature increases, the Q × f values of the ceramics increases first and reached a maximum at 1175 °C. While the sintering temperature reaches 1200 °C, the Q × f values decreased. The trend of the Q × f values of $(1-x)$ $Li_2Zn_3Ti_4O_{12}$–x $CaTiO_3$ (3 wt% ≤ x ≤ 7 wt%) ceramics are match well with bulk density values. As known, the Q × f values are not only affected by the lattice vibrational modes but also affects by the second phase, pores, impurities, and density etc. extrinsic factors [18, 19]. While for the same temperature, as the x increases from 3 to 7 wt%, the Q × f values of the ceramics decreases, which owing to the large difference in the Q × f values of $Li_2Zn_3Ti_4O_{12}$ (Q × f ~ 106,700 GHz) and $CaTiO_3$ (Q × f ~ 3600 GHz). In this works, therefor, densification and second phase are plays important roles in controlling the the Q × f values of $(1-x)$ $Li_2Zn_3Ti_4O_{12}$–x $CaTiO_3$ (3 wt% ≤ x ≤ 7 wt%) ceramics. A maximum Q × f value of 61,490 GHz could be achieved for the 0.94 $Li_2Zn_3Ti_4O_{12}$–0.06 $CaTiO_3$ ceramic sintered at 1175 °C for 4 h.

Figure 9 illustrates the τ_f values of the $(1-x)$ $Li_2Zn_3Ti_4O_{12}$–x $CaTiO_3$ (3 wt% ≤ x ≤ 7 wt%)

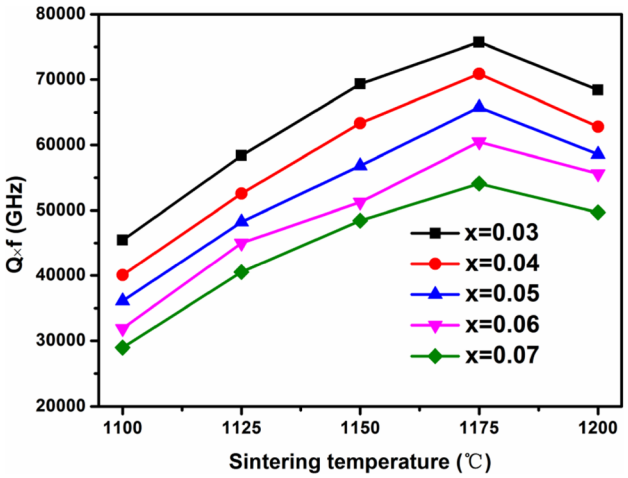

Fig. 8 Variation in the Q×f values of $(1-x)$ $Li_2Zn_3Ti_4O_{12}$–x $CaTiO_3$ (3 wt% ≤ x ≤ 7 wt%) ceramics as a function of the sintering temperature

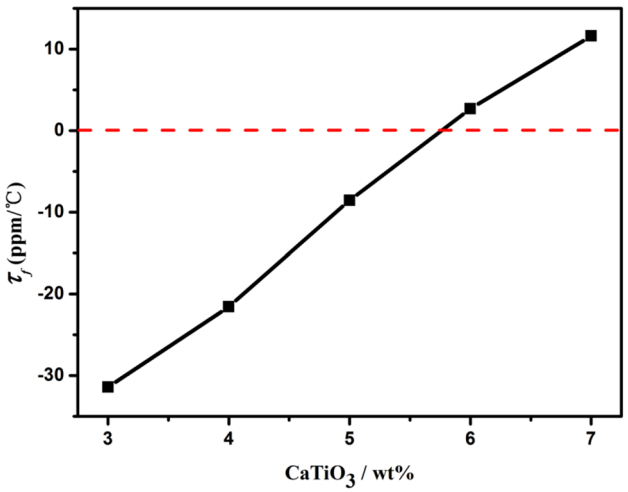

Fig. 9 The τ_f values of $(1-x)$ $Li_2Zn_3Ti_4O_{12}$–x $CaTiO_3$ (3 wt% ≤ x ≤ 7 wt%) ceramics sintered at 1175 °C for 4 h

ceramics sintered at 1175 °C for 4 h. As shown, with the x variation from 3 to 7 wt%, the τ_f values increased from − 31.2 ppm/°C to + 11.6 ppm/°C. Generally speaking, the composition, additives, and second phases are the main factors for the τ_f values of microwave dielectric ceramics [20]. By increasing x, the τ_f values of $(1-x)$ $Li_2Zn_3Ti_4O_{12}$–x $CaTiO_3$ (3 wt% ≤ x ≤ 7 wt%) ceramics varied toward positive direction. In addition, according to the mixing rules, the τ_f values were compensated. Therefor, a near-zero τ_f values of $(1-x)$ $Li_2Zn_3Ti_4O_{12}$–x $CaTiO_3$ (3 wt% ≤ x ≤ 7 wt%) ceramics could be obtained by doping an appropriate content of $CaTiO_3$. When the $CaTiO_3$ amount is 6 wt%, a near-zero τ_f value with + 2.68 ppm/°C obtained.

4 Conclusions

In this work, $CaTiO_3$ as a τ_f compensation material added to $Li_2Zn_3Ti_4O_{12}$ ceramic to form a new ceramics systems of $(1-x)$–x $CaTiO_3$ (3 wt% ≤ x ≤ 7 wt%) were investigated systematic. The XRD and EDS results demonstrated that the $(1-x)$ $Li_2Zn_3Ti_4O_{12}$–x $CaTiO_3$ (3 wt% ≤ x ≤ 7 wt%) compositions ceramics shown a mixture of two phases, $Li_2Zn_3Ti_4O_{12}$ and $CaTiO_3$ phase. The SEM micrographs shown that with the $CaTiO_3$ increased, the average grain size of $(1-x)$ $Li_2Zn_3Ti_4O_{12}$–x $CaTiO_3$ (3 wt% ≤ x ≤ 7 wt%) composition ceramics decreased. Moreover, the microwave dielectric properties of the composition ceramics can be effectively controlled by varying the $CaTiO_3$ contents. The values of the ε_r and τ_f were found to increase, but the Q × f values were found to decrease when the $CaTiO_3$ contents increased from 3 to 7 wt%. Typically, a new temperature stable microwave dielectric material of 0.94 $Li_2Zn_3Ti_4O_{12}$–0.06 $CaTiO_3$ with excellent microwave dielectric properties of ε_r = 21.7, Q × f = 61,490 GHz, and τ_f = + 2.68 ppm/°C were obtained when sintered at 1175 °C for 4 h.

Acknowledgements This research did not receive any specific grant from funding agencies in the public, commercial, or not-for-profit sectors. The authors would like to express thanks to Huixing Lin for the support in microwave dielectric properties test and their technical support.

References

1. M.T. Sebastian, H. Wang, H. Jantunen, Curr. Opin. Solid State Mater. Sci. **20**, 151–170 (2016)
2. T.Y. Xie, L.Z. Zhang, H.S. Ren, J. Mater. Sci.: Mater. Electron. **28**, 13705–13709 (2017)
3. G.J. Shu, Q. Zhang, F. Yang, J. Mater. Sci.: Mater. Electron. **29**, 17008–17015 (2018)
4. J. Iqbal, H. Liu, H. Hao, Ceram. Int. **43**, 14156–14160 (2017)
5. S. George, M.T. Sebastian, J. Am. Ceram. Soc. **93**, 2164–2166 (2010)
6. L. Fang, D.J. Chu, H. Zhou, J. Alloys Compd. **509**, 1880–1884 (2011)
7. H. Zhou, X. Liu, X. Chen, J. Eur. Ceram. Soc. **32**, 261–265 (2012)
8. H. Zhou, X. Liu, X. Chen, Mater. Chem. Phys. **137**, 22–25 (2012)
9. H. Zhou, X. Liu, X. Chen, Mater. Res. Bull. **47**, 1278–1280 (2012)
10. C.H. Su, C.L. Huang, J. Alloys Compd. **678**, 102–108 (2016)
11. R.C. Kell, A.C. Greenham, G.C.E. Olds, J. Am. Ceram. Soc. **56**, 352–354 (1973)
12. S. Wu, K.X. Song, P. Liu, J. Am. Ceram. Soc. **98**, 1842–1847 (2015)
13. X. Zhou, L. Xue, H. Sun, J. Mater. Sci.: Mater. Electron. **29**, 643–649 (2018)
14. C.L. Huang, J.Y. Chen, B.J. Li, J. Alloys Compd. **509**, 4247–4251 (2011)

15. L. Li, M. Zhang, Q. Liao, J. Alloys Compd. **531**, 18–22 (2012)
16. L. Li, J. Ye, S. Zhang, J. Alloys Compd. **648**, 184–189 (2015)
17. J.S. Wei, P. Liu, H.X. Lin, J. Alloys Compd. **689**, 81–86 (2016)
18. J. Song, K. Song, J. Wei, J. Am. Ceram. Soc. **101**, 244–251 (2018)
19. L. Hao, G.J. Shu, F.C. Meng, Ceram. Int. **44**, 13139–13144 (2018)
20. L. Li, Z. Gao, Y. Liu, Mater. Lett. **140**, 5–8 (2015)